Optical Flow Dynamic Measurements with High-Speed Camera on a Small-Scale Steel Frame Structure

Cecilia Rinaldi[1(✉)], Jacopo Ciambella[2], Monica Moroni[3], and Vincenzo Gattulli[2]

[1] DICEAA, University of L'Aquila, via G. Gronchi 18, 67100 L'Aquila, Italy
cecilia.rinaldi@graduate.univaq.it
[2] DISG, Sapienza – University of Rome, via Eudossiana 18, 00184 Rome, Italy
{jacopo.ciambella, vincenzo.gattulli}@uniromal.it
[3] DICEA, Sapienza – University of Rome, via Eudossiana 18, 00184 Rome, Italy
monica.moroni@uniromal.it

Abstract. The tremendous advances in high-resolution and high-speed cameras have allowed improving optical measurement techniques enabling extraction of dynamic characteristics of vibrating structures. These techniques turned out to be particularly useful for vibration observations as they are contactless, and they do not interfere with the structural response (as is the case of accelerometers installed on a light-weight set-up, with non-negligible additional masses). The paper reports the results of an experimental campaign, carried out to verify the accuracy of the dynamic displacements measurement obtained with a high-speed camera and the Hybrid Lagrangian Particle Tracking software, a software based on the solution of the Optical Flow equation. The experimental setup includes a 4-dof small-scale steel frame structure excited on a shaking table, a high-speed camera able to record images of the motion and five accelerometers. From images, a two-dimensional moving field is recorded, and the absolute and relative displacements are determined. Confidence in the novel developed measuring methodology is determined by direct comparison with acceleration measurements which confirm that the image analysis measurements turned out to be sufficiently accurate for damage identification purposes.

Keywords: High-speed camera · Feature tracking · Image analysis dynamic measurements · Structural Health Monitoring

1 Introduction

Structural Health Monitoring (SHM) allows the actual state and characteristics of new and existing structures to be assessed. As it be, it is a powerful tool to monitor the state of the structures during the construction, execute final tests, verify the safety condition and eventually propose maintenance actions. Advances in sensing technologies and data processing techniques are making a huge contribution to SHM with the development of sophisticated monitoring and communication systems able to support an aware decision making [1]. For such a task, it is useful to measure some physical parameters which can

A. Carcaterra et al. (Eds.): AIMETA 2019, LNME, pp. 1543–1555, 2020.
https://doi.org/10.1007/978-3-030-41057-5_125

give information on structural loads, features and responses. Mainly, one is led to measure the acceleration response due to the easiness of the experimental setup needed; on the other hand, displacements are a good indicator of the structural performance, as they can be used to extract strains and stresses [2]. The knowledge of the deformations magnitude would allow the operating conditions to be examined, whilst constructing time-varying deformation patterns from discrete displacement measurements provides different information about the state od structures [3].

Displacements can be obtained from measured accelerations and strains with numerical integration algorithms [4], but this procedure can generate errors due to the uncertainty on the initial conditions and the inevitable presence of noise [5]. To directly measure displacements, contact and non-contact sensors are usually employed. Contact sensors include the Linear Variable Differential Transformer (LVDT) [6], that needs to be attached to a stationary reference point of the structure. Global position system (GPS), laser vibrometer and radar interferometry system, are instead non-contact sensors. These devices have the advantage of not being required to be attached to the structure under monitoring, hence they do not interfere with its structural response, but at the same time they have drawbacks: GPS sensors have limited measurement accuracy (5–10 mm errors); the laser vibrometer has a limited measurement distance; and the interferometric radar system requires reflecting surfaces mounted on the structure [7].

Optical displacement measurements are vision-based methods that are catching on in the field of SHM due to their favorable properties since they are contactless, non-destructive, highly precise, immune to electromagnetic interference, and large-range and multiple-target measurements [8]. Furthermore, the spread of optical measures in SHM has been encouraged also by the continuous progress of high-quality cameras and computer vision (CV) algorithms [3, 8]. Most researchers use a digital image correlation (DIC) algorithm [9] to obtain image-based displacement measurements, by means of also manual markers to improve the accurateness of the method. A target-free approach was proposed in [10] for vision-based structural system identification using Kanade-Lucas-Tomasi (KLT) tracking algorithm and Shi-Tomasi corners. In [11], physical markers used for target localization are replaced with virtual markers (feature points, such as textures or other unique surface characteristics of the structure) that are extracted from video frames by robust feature detection algorithms.

Within the broad framework described above, the aim of this work is to demonstrate the accuracy of the image-based dynamic displacement measurements. Dynamic tests were conducted on a small-scale steel structure and two acquisition systems (accelerometers and a high-speed camera) were used to measure the structural response.

In Sect. 2, the algorithm used to obtain the displacements from the image analysis is briefly described, while, in Section, 3 the experimental tests performed, and the results obtained are discussed.

2 Particle Tracking Algorithm

The image sequences were processed by the Hybrid Lagrangian Particle Tracking (HLPT [12]) algorithm to obtain the trajectories and the displacement, velocity and acceleration fields of feature points. The HLPT algorithm is based on the solution of the

optical flow equation and selects areas of each image where strong brilliance gradients exist. Such areas can be associated to feature points and are good features to track from frame to frame. Once the feature points have been identified, the algorithm calculates the coordinates of their barycenter and reconstructs their trajectories, calculating their displacement in the subsequent frames.

Image processing was achieved in two steps: (1) particle detection and temporal tracking via HLPT to isolate particles and track them in consecutive frames; (2) post-processing to obtain the relevant flow parameters.

Through the solution of the image intensity conservation equation, a set of positions, associated with the displacement vector predictor, for which the optimization problem is well-posed, is detected. Those positions, also defined as features are then associated to the centroid coordinates using two 1D Gaussian functions built around the integer position of the local maximum of the intensity value of each detected feature. The set of validated particle image locations and the displacement vector predictor associated to the particle, given by the approximated solution of the optical flow equation, are finally used as input data for the tracking algorithm. To identify successive positions of the same particle and thus extract the displacement of that particle along its trajectory, the nearest neighbor principle was employed. Among the candidates, that with the minimum Eulerian distance from the position determined with the displacement predictor was selected. However, this method differs from the 'classical' nearest neighbor one because the solution of the assignment problem is strengthened by using the displacement vector predictor; as such, it does not suffer from the typical drawbacks of the 'classical' nearest neighbor, such as being erroneously influenced by fast moving particles with respect to the mean inter-particle distance.

3 Experiments

3.1 Experimental Setup

Tests have been performed at the "Laboratory of Materials and Structures" of Sapienza, University of Rome (Italy).

The structure is a spatial model of a 4-story shear type steel (S235) structure, shown in Fig. 1a. The frame was designed to have the first frequency above the lower frequency at which the electrodynamic shaker could be reliably controlled, which in the present case was 5 Hz. Its height is 800 mm, the plan is squared (300 × 300 mm), the cross section of columns is rectangular (50 × 4 mm) and the one of beams is L-shaped (50 × 50 × 4 mm).

As shown in Fig. 1a, sand (0.3–0.5 mm diameter) was used to create the features to be tracked with the Particle Tracking (PT) algorithm. We used both white and yellow sand to understand which color lends itself best to be tracked. After processing the results, we found out that the color of the sand is irrelevant.

The structure was subject both to a random and an impulsive excitation in the x-direction. The random test was carried out by imposing a motion at the base of the structure and by recording the accelerations. The test was based on an artificial excitation induced by a one-dimensional electrodynamic shaker. The shaker used is the

Dongling GT700M (slip plate dimension 700 × 700 × 45 mm^3, dynamic range ± 10.3 g, moving mass 58 kg, frequency range 5–2000 Hz). The signal sent to the structure was random, not periodic and continuous over time, with peaks having a Gaussian probability distribution. Its single registration contains random amplitude and phase data at each frequency. On average, however, the spectrum is flat and continuous, therefore it contains almost constant energy for all frequencies.

The impulsive test consisted in applying an instantaneous force with an instrumented hammer, used to hit the structure at the top floor. The instrumented hammer was the PCB Piezotronics Modally Tuned ICP (Integrated Circuit Piezoelectric) model, 086C20, sensitivity: 0.23 mV/N, measurement range: ± 22240 N pk, hammer mass: 5.5 kg and equipped with a resistant force sensor integrated in the swing surface of the hammer.

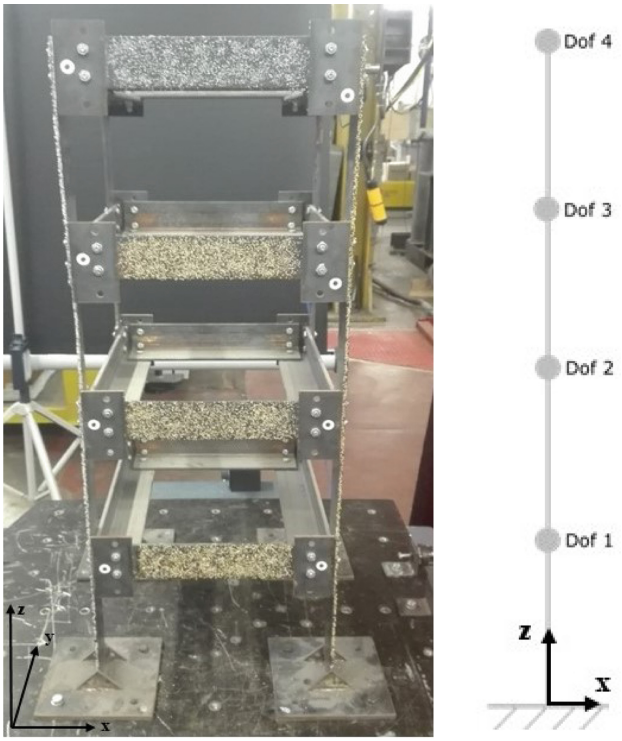

a) b)

Fig. 1. (a) Small-scale steel frame structure used for the experimental test; 0.3–0.5 mm diameter sand has been attached on the beams and on the columns to create the features to be tracked with the PT algorithm. (b) 4-dof simplified model of the shear-type frame structure.

Two acquisition systems were used to record both accelerometric and image-based measurements. The first acquisition system consisted of 6 channels, one of which is

dedicated to the hammer force sensor, 4 to the accelerometers placed one per floor and one placed at the base. The accelerometers used in these tests are piezoelectric PCB 393A03 (sensitivity 1000 mV/g, dynamic range ±5 g, mass 210 g, frequency range 0.5–2000 Hz) and PCB 352C33 (sensitivity 100 mV/g, dynamic range ±5 g, mass 5.8 g, frequency range 0.5–10000 Hz). Accelerometers of the first type were mounted at the base and on the floors 1, 2, 3, while the second type on the 4th floor. They were connected to the structure by means of metal plates and small magnets. The accelerometers used are from PCB Piezotronics which produces robust and precision accelerometers to meet accurate measurements of vibration, shock, acceleration and movement for monitoring, control and test applications. In particular, they are single-axis ICP integrated circuit sensors and powered by the acquisition system itself. These outputs provide a voltage signal proportional to the acceleration that generated it. The constant of proportionality is the sensitivity. Signals are acquired using the LabVIEW software produced by National Instruments.

The second acquisition system includes a video camera and a digital recorder of IO Industries. The camera is the Flare 12M125xCL, a high resolution, high-speed area scan camera designed for a broad range of applications, such as automated inspection, high speed motion analysis, research imaging, specialty video production. The sensor type is CMOS w. global electronic shutter, the sensor size (resolution) is 4096 × 3072 and the pixel size 5.5 x 5.5 μm. Other characteristics of the camera are: dynamic range/sensitivity 60 dB, 4.64 V/lux.s, output format camera link, color monochrome, frame rate (full resolution) 124 fps (8-bit) and 100 fps (10-bit). The lens mount is F-mount and the focal lens is NIKO AF-Nikkor 28 mm f/2.8D. The digital recorder is the CORE2CLPLUS IO DVR, Core 2, supporting camera link connection up to 4 base inputs and up to 2 full inputs and it includes the CoreView, a software that displays live video during recording and allows to configure and to manage the camera and the video recorder. Finally, four 240 GB video storage module (VIDIOMOD240) is used. The camera connects to the Core with 4 Camera Link cables COMPONENT MDR Male Straight Molded to MDR Male Straight Molded 3 m length and the Core connects easily to laptops or PCs via USB 3.0 (as shown in Fig. 2). In Fig. 3, a sketch of the experimental setups and acquisitions systems is reported; the camera is installed in front of the structure to capture images in the plane $x - z$ (motion plane).

Fig. 2. Image-based acquisition system: high-speed camera, core and PC.

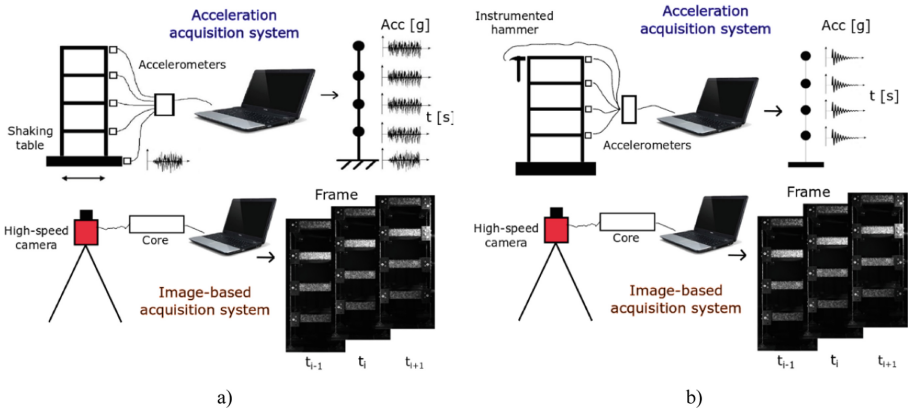

Fig. 3. Sketch of the experimental setups and acquisition systems: (a) random excitation with shaking table; (b) impulsive excitation with instrumented hammer.

The camera parameters (such as frame rate and time exposure) were set according to the dynamic characteristics of the structure and to the light conditions of the surrounding environment. From a 4-dof theoretical model of the shear-type structure (Fig. 1b), we derived the main dynamic properties reported in Table 1. To identify the four frequencies listed in this table through experimental data, we set the camera frame rate to 200 fps. The time exposure depends on the frame rate and the light conditions; in this case, we set it to 1250 μs with the aim to avoid overexposed images. Furthermore, thanks to these modal properties calculated, we were able to calibrate the random test, adopting a white noise, flat in the range of frequencies involving the structure, 8–100 Hz.

Table 1. Dynamic properties of the 4-dof shear-type frame structure.

Mode	Frequency [Hz]
1	15.92
2	43.72
3	72.27
4	82.61

3.2 Results

The main effort of this work is the evaluation of the dynamic displacements retrieved with the PT algorithm. This algorithm returns the trajectories of feature points, created by attaching white and yellow sand on all beams and columns surfaces, so we could

sample different points along the whole structure. In this way, with the image acquisition system we got many more measurement points than the accelerometer system acquisition ones that provide only 4 measures. In this case, we extracted 24 measurement points from image analysis measurements: a representative point of each floor and 20 points along the column. As we show below, a large number of measurement points allows a more complete picture of the structural behavior and a better description of the mode-shapes.

The trajectory of the j-th feature point contains its position $(x^j(t), z^j(t))$ in pixel in each image/frame (each frame corresponds to the time instant t). The displacement u in the x-direction with respect to the initial position of the feature is calculated as:

$$u^j(t_i) = \left(x^j(t_i) - x^j(t_0)\right)L/l,$$

where L is the physical length of the object on the motion plane, and l is the length in pixel of its corresponding image part. The velocity and the acceleration in x-direction of the j-th feature are respectively:

$$\dot{u}^j(t_i) = \frac{u^j(t_{i+1}) - u^j(t_i)}{\Delta t} \text{ and } \ddot{u}^j(t_i) = \frac{\dot{u}^j(t_{i+1}) - \dot{u}^j(t_i)}{\Delta t}, \text{ with } \Delta t = \frac{1}{fps} = \frac{1}{200}\text{s}$$

where Δt is the inverse of the acquisition rate. In the following, we report the comparison among accelerometer and image-based measurements of the response of the structure to the random (Fig. 4) and impulsive (Fig. 5) excitation. We compared the floor accelerations measured with accelerometers and the accelerations calculated as the second derivative of the displacements.

We applied the Frequency Domain Decomposition (FDD) [13] to both measurement systems to detect the first four frequencies (Table 2) and mode-shapes (Fig. 6) of the structure.

Table 2. Frequencies [Hz] of the shear-type frame structure detected with both measurement systems.

Mode	Accelerometers	Images	Δ [%]
1	14.92	14.99	0,47
2	43.90	43.58	−0,73
3	70.94	71.14	0,28
4	82.64	82.98	0,41

Finally, with the addition of a steel bracing on the structure (Fig. 7b), we modified its behavior to study the two states of the structure through the comparison of the frequencies (Tables 3 and 4) and mode-shapes (Figs. 7c and 9). As is usual in damage identification and model updating procedures [14], we evaluated also the Relative Difference (RD) [15] and COordinate Modal Assurance Criterion (COMAC) [16], reported in Figs. 8 and 10.

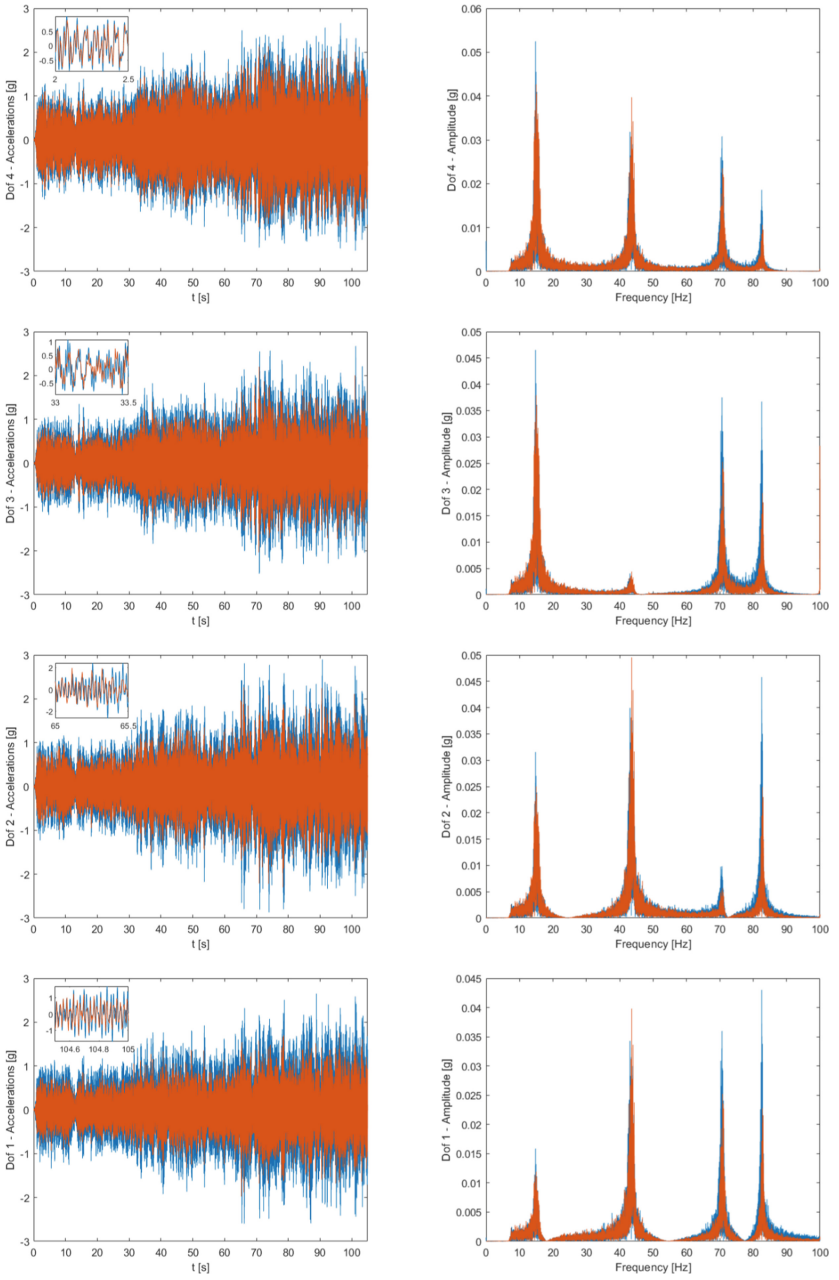

Fig. 4. Comparison among accelerometers (blue) and image analysis (orange) measurements of the response of the structure to the random excitation. The acceleration responses of the 4 floors are reported in the time domain (on the left side) and in the frequency domain (on the right side) .

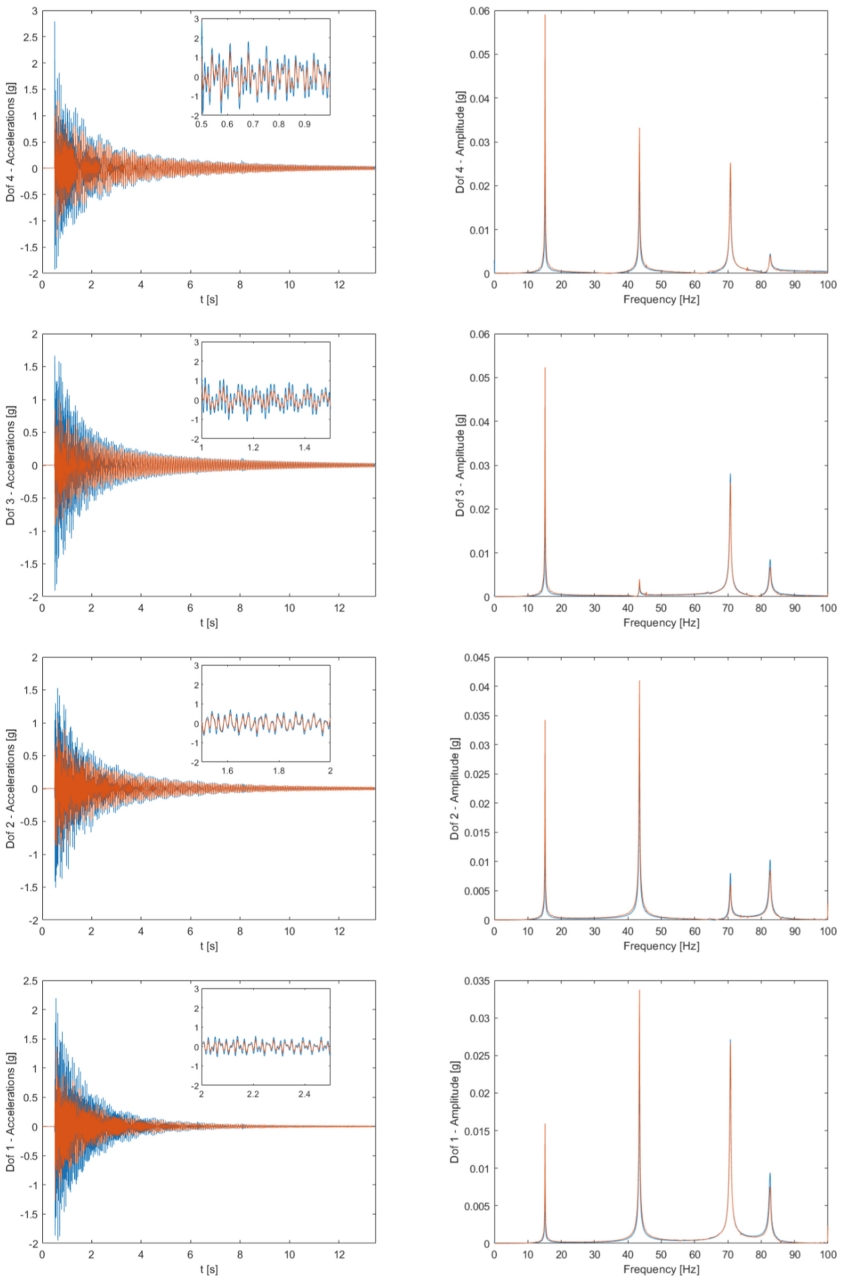

Fig. 5. Comparison among accelerometers (blue) and image analysis (orange) measurements of the response of the structure to the impulsive excitation. The acceleration responses of the 4 floors are reported in the time domain (on the left side) and in the frequency domain (on the right side) .

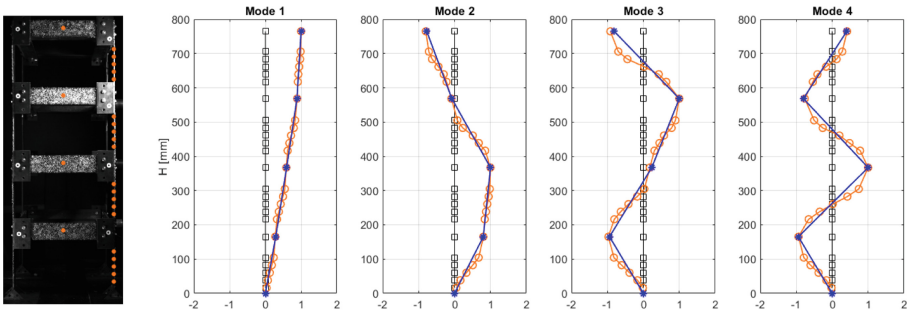

Fig. 6. Mode-shapes comparison: (a) Image-based acquisition system measurements points. (b) Accelerometers (blue, 4 measurements points) vs image analysis (orange, 24 measurements points) .

Table 3. Frequencies [Hz] of the two states of structure evaluated with image measurements.

Mode	Without steel bracing	With steel bracing	Δ [%]
1	14.99	17.26	15.15
2	43.58	55.00	26.22
3	71.14	72.88	2.44

Table 4. Frequencies [Hz] of the two states of structure evaluated with accelerometers.

Mode	Without steel bracing	With steel bracing	Δ [%]
1	14.92	17.23	15.49
2	43.90	54.90	25.05
3	70.94	72.78	2.60

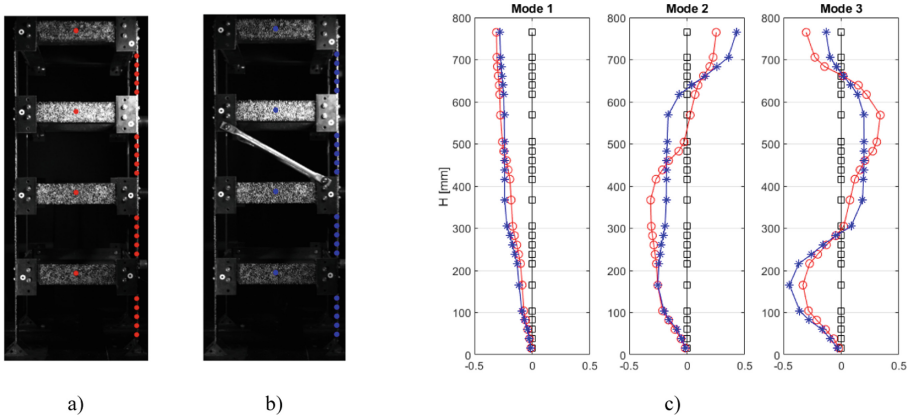

Fig. 7. Comparison of two states of the structure: (a) without steel bracing. (b) with steel bracing. (c) Mode-shapes comparison of the structure without (red) and with (blue) steel bracing, calculated with image analysis .

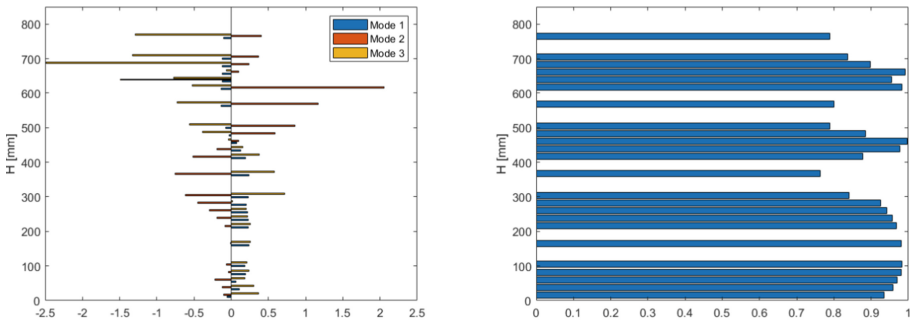

Fig. 8. Comparison of two states of the structure, with and without the steel bracing. (a) RD and (b) COMAC calculated with image analysis.

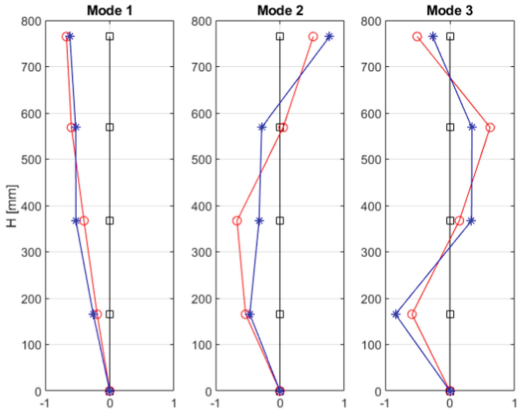

Fig. 9. Mode-shapes of the structure without (red) and with (blue) steel bracing, calculated with accelerometers measurements .

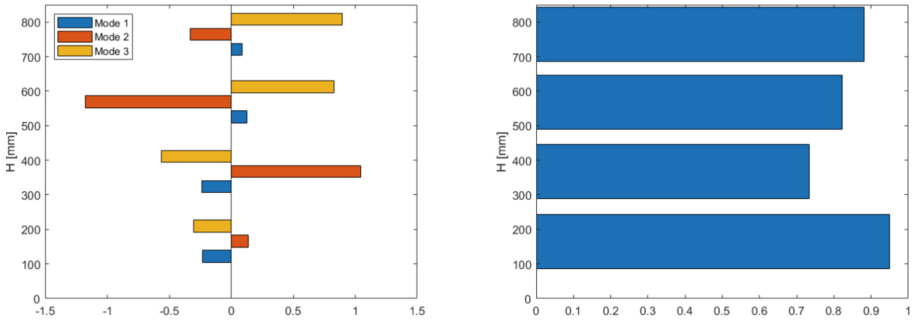

Fig. 10. Comparison of two states of the structure, with and without the steel bracing. (a) RD and (b) COMAC calculated with accelerometers measurements.

4 Conclusions

In this work, an image-analysis dynamic displacement measurement technique was used to extract the modal properties (modal frequencies and mode shapes) of a small-scale prototype structure. The results of this analysis were compared to standard accelerometer measurements. The optical technique provides a much larger number of points at which the displacement was extracted, 24 in the present case compared to 4 for the accelerometer measurements. As such, a more accurate evaluation of the mode shape was possible with the further advantage of being able to estimate accurately the differences of the structural behavior in two states (e.g., in this case, without and with a steel bracing). Accordingly, the image analysis can be a valid support to damage identification (which requires a comparison between two system states), because it can allow to locate accurately the position of the damage.

Acknowledgments. These experimental results are part of a project that has received funding from the Research Fund for Coal and Steel under grant agreement No 800687.

References

1. Fujino, Y., Siringoringo, D.M., Abe, M.: The needs for advanced sensor technologies in risk assessment of civil infrastructures. Smart Struct. Syst. **5**(2), 173–191 (2009)
2. Wu, L., Casciati, F.: Local positioning systems versus structural monitoring: a review. Struct. Control Health Monit. **21**, 1209–1221 (2014)
3. Xu, Y., Brownjohn, J.: Review of machine-vision based methodologies for displacement measurement in civil structures. J. Civ. Struct. Health Monit. **8**, 91–110 (2018)
4. Park, K., Kim, S., Park, H., Lee, K.: The determination of bridge displacement using measured acceleration. Eng. Struct. **27**, 371–378 (2005)
5. Li, J., Hao, H., Fan, K., Brownjohn, J.: Development and application of a relative displacement sensor for structural health monitoring of composite bridges. Struct. Control Health Monit. **22**, 726–742 (2015)
6. Thomsen IV, J.H., Wallace, J.W.: Displacement-based design of slender reinforced concrete structural walls - experimental verification. J. Struct. Eng. **130**(4), 618–630 (2004)
7. Feng, D., Feng, M., Ozer, E., Fukuda, Y.: A vision-based sensor for noncontact structural displacement measurement. Sensors **15**, 16557–16575 (2015)
8. Ye, X., Dong, C.Z., Liu, T.: A review of machine vision-based structural health monitoring: methodologies and applications. J. Sensors **2016**, 1–10 (2016)
9. Yoneyama, S., Ueda, H.: Bridge deflection measurement using digital image correlation with camera movement correction. Mater. Trans. **53**(2), 285–290 (2012)
10. Yoon, H., Elanwar, H., Choi, H., Golparvar-Fard, M., Spencer Jr., B.F.: Target-free approach for vision-based structural system identification using consumer-grade cameras. Struct. Control Health Monit. **23**, 1405–1416 (2016)
11. Dong, C.Z., Celik, O., Catbas, F.N.: Marker-free monitoring of the grandstand structures and modal identification using computer vision methods. Struct. Health Monit. **18**, 1491–1509 (2018)
12. Moroni, M., Cicci, A., Bravi, M.: Experimental investigation of a local recirculation photobioreactor for mass cultures of photosynthetic microorganisms. Water Res. **52**, 29–39 (2014)

13. Brincker, R., Zhang, L., Andersen, P.: Modal identification of output-only systems using frequency domain decomposition. Smart Mater. Struct. **10**, 441–445 (2001)
14. Foti, D., Gattulli, V., Potenza, F.: Output-only identification and model updating by dynamic testing in unfavourable conditions of a seismically damaged building. Comput. Aided Civ. Infrastruct. Eng. **29**, 659–675 (2014)
15. Fox, C.H.J.: The location of defects in structures. A comparison of the use of natural frequency and mode shape data. In: 10th International Modal Analysis Conference, IMAC (1992)
16. Lieven, N.A.J., Ewins, D.J.: Spatial correlation of mode shapes, the coordinate modal assurance criterion (COMAC). In: 6th International Modal Analysis Conference, IMAC (1988)